Review of Scientific Instruments

W-band millimeter-wave back-scattering system for high wavenumber turbulence measurements in LHD

Cite as: Rev. Sci. Instrum. **92**, 043536 (2021); https://doi.org/10.1063/5.0043474
Submitted: 08 January 2021 • Accepted: 01 April 2021 • Published Online: 13 April 2021

T. Tokuzawa, K. Tanaka, T. Tsujimura, et al.

Review of Scientific Instruments ARTICLE scitation.org/journal/rsi

W-band millimeter-wave back-scattering system for high wavenumber turbulence measurements in LHD

Cite as: Rev. Sci. Instrum. 92, 043536 (2021); doi: 10.1063/5.0043474
Submitted: 8 January 2021 • Accepted: 1 April 2021 •
Published Online: 13 April 2021

T. Tokuzawa,[1,2,a)] K. Tanaka,[1,3] T. Tsujimura,[1] S. Kubo,[1,4] M. Emoto,[1] S. Inagaki,[3] K. Ida,[1,2] M. Yoshinuma,[1] K. Y. Watanabe,[1,4] H. Tsuchiya,[1] A. Ejiri,[5] T. Saito,[6] K. Yamamoto,[6] and LHD Experiment Group[1,b)]

AFFILIATIONS

[1] National Institutes of Natural Sciences, National Institute for Fusion Science, Toki 509-5292, Japan
[2] SOKENDAI (The Graduate University for Advanced Study), 322-6 Oroshi, Toki-city 509-5292, Japan
[3] Research Institute for Applied Mechanics, Kyushu University, Kasuga 816-8580, Japan
[4] Department of Energy Engineering and Science, Nagoya University, Furo-cho, Chikusa-ku, Nagoya 464-8601, Japan
[5] Graduate School of Frontier Sciences, The University of Tokyo, Kashiwa 277-8561, Japan
[6] Research Center for Development of Far-Infrared Region, University of Fukui, Bunkyo 3-9-1, Fukui 910-8507, Japan

Note: Paper published as part of the Special Topic on Proceedings of the 23rd Topical Conference on High-Temperature Plasma Diagnostics.
[a)] **Author to whom correspondence should be addressed:** tokuzawa@nifs.ac.jp
[b)] Author list of Y. Takeiri, T. Morisaki *et al.*, Nucl. Fusion **57**, 102023 (2017).

ABSTRACT

A 90 GHz W-band millimeter-wave back-scattering system is designed and installed for measuring electron scale turbulence ($k_\perp \rho_s \sim 40$). A metal lens relay antenna is used for in-vessel beam focusing, and a beam diameter of less than 40 mm is achieved in the plasma core region. This antenna can be steered at an angle of $159^\circ \pm 6^\circ$, which almost covers the plasma radius. The estimated size of the scattering volume is ~105 mm at the edge and 135 mm at the core, respectively. A 60 m corrugated waveguide is used to achieve a low transmission loss of ~8 dB. A heterodyne detection system for millimeter-wave circuits with probing power modulation can distinguish the scattered signal from background noise.

I. INTRODUCTION

Multi-scale turbulence interaction, especially mixed micro-scale turbulence phenomenon, which includes both ion and electron scale turbulences, is of interest[1] in the high temperature plasma confinement study at present, and there are many theoretical studies.[2–8] Simultaneous measurements of each electron scale turbulence and ion scale turbulence are required. However, the measurement of turbulence, especially on the electron scale, is state-of-the-art because this observation requires very high spatial and temporal resolutions. There are a few previous studies of this diagnostic in tokamaks such as NSTX,[9,10] DIII-D,[11] KSTAR,[12] MAST,[13] and NSTX-U.[14] We have developed and installed this electron scale turbulence diagnostic to the Large Helical Device (LHD[15]) plasma, and this is the first report for the application to the helical device to the author's knowledge. In addition, LHD has several ion-scale turbulence diagnostics, such as CO_2 laser used phase constant imaging (PCI),[16] a microwave Doppler reflectometer,[17] and beam emission spectroscopy (BES).[18] The ion scale turbulence observations have been compared with the gyrokinetic simulation (GKV[19,20]) results.[21–23] The introduction of this electron scale turbulence measurement will allow for a more detailed comparative study.

In order to measure an electron-scale turbulence such as electron temperature gradient (ETG) driven mode, which has a high wavenumber ($k_\perp \rho_s \sim 40$ and $k_\perp \sim 40\,\mathrm{cm}^{-1}$), a millimeter-wave

back-scattering system is one of the suitable candidates, where $k_\perp$ is the fluctuation wavenumber perpendicular to the magnetic field and ρ_s is the ion gyroradius at the electron temperature. When the electromagnetic wave is launched to the turbulent plasma, a scattered wave that satisfies the Bragg relationship $k = 2k_i \sin(\theta_s/2)$ is generated.[24] Here, k_i is the local wavenumber of the probing beam and θ_s is the scattering angle. To measure higher wavenumbers of $k_\perp \sim 40\ \mathrm{cm}^{-1}$, one can choose either forward-scattering of terahertz waves or back-scattering of W-band millimeter waves, as shown in Fig. 1. In general, there are two types of scattering conditions. One is collective, and the other is non-collective scattering. Considering the current situation, the scattering parameter (so-called Salpeter parameter) $\alpha = (k_\perp \lambda_{De})^{-1}$ is calculated under several plasma conditions of temperature and density, as shown in Fig. 2. Here, λ_{De} is the electron Debye length. The electron density is higher than $1 \times 10^{19}\ \mathrm{m}^{-3}$ in the usual LHD plasma experiments; thus, the diagnostic region is almost in $\alpha > 1$. This means that the scattering signal is collective, and the scattering signal originates from the correlated density fluctuation $\tilde{n}_e$ behavior as in the following equation:[12,24]

$$P_s = \frac{1}{4} r_0^2 |\tilde{n}_e|^2 \lambda_i^2 L^2 P_i,$$

where P_s is the scattered power, r_0 is the classical electron radius, λ_i is the probing wave's wavelength, L is the scattering length, and P_i is the probing wave power.

Considering the installation of a millimeter-wave scattering system on the LHD, W-band 90 GHz is suitable as a probing frequency. There is no electron cyclotron resonance layer in the plasma confinement region in the line of sight, as shown in Fig. 3. When we use the ordinary mode (O-mode) propagation in the plasma, we can access the plasma core region. However, the plasma center is located

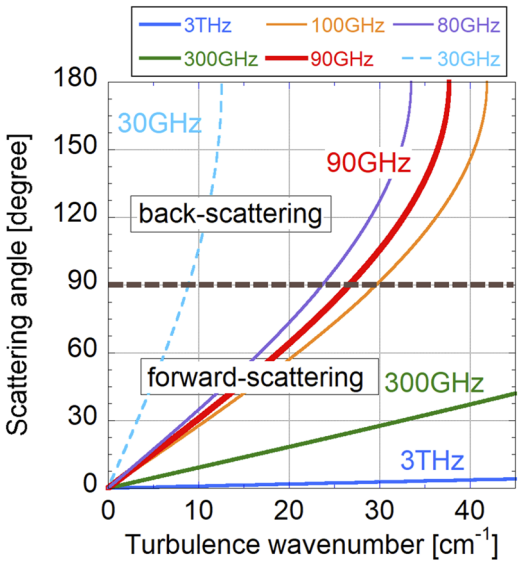

FIG. 1. Bragg relationship between the scattering angle and the turbulence wavenumber as a function of launching frequency. Here, an angle greater than 90° implies back-scattering.

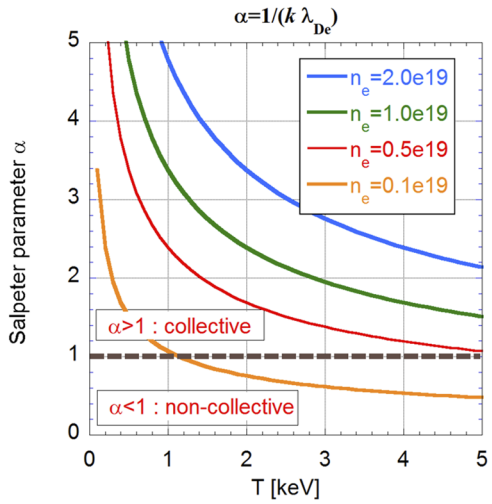

FIG. 2. Salpeter parameter α as a function of temperature and electron density. Here, the wavenumber k is calculated as $k = 40\ \mathrm{cm}^{-1}$, and $\alpha > 1$ means that the scattering condition is collective.

~3 m away from the vacuum window because of the complicated LHD vacuum chamber. We need the focusing optics to be precise for small scale turbulence observation. For this aim, we developed the in-vessel focusing antenna. In addition, the complex magnetic

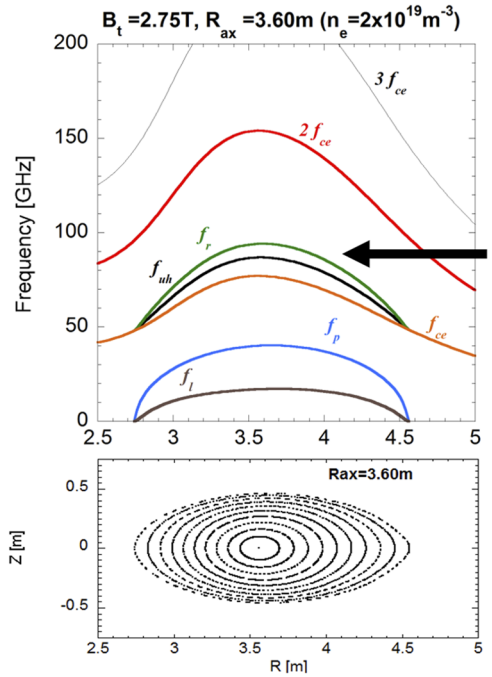

FIG. 3. Radial profiles of characteristic frequencies (upper) and magnetic flux surfaces in the horizontal plasma cross section (bottom). Here, f_{ce}, 2 f_{ce}, 3 f_{ce}, f_p, f_r, f_l, and f_{uh} mean the fundamental, second harmonic, and third harmonic electron cyclotron frequencies, electron plasma frequency, right-hand cutoff frequency, left-hand cutoff frequency, and upper hybrid frequency, respectively.

structure generates stray light, especially electron cyclotron emission (ECE), which plays an important role in the background noise.

In this paper, we describe the in-vessel focusing antenna and the millimeter wave circuits of back-scattering system and its characteristics as follows.

II. METAL LENS RELAY ANTENNA

Since the turbulence structure is small and the observation position in the plasma core region is located ~3 m away from the vacuum window, the probing wave beam must be focused. In addition, the limited space around the viewing window precludes the use of large focusing optics. Furthermore, beam steering capability is also required because of the requirement to measure the radial structure of the turbulence. Figure 4 shows the cross section of the observation line of sight of the back-scattering system. A possible method is the in-vessel focusing optics. For these aims, the metal lens antenna is applied as an in-vessel focusing antenna. This antenna is composed of a conical horn and two lenses arranged in a co-linear configuration, as shown in Fig. 5. One lens is a bi-concave shaped lens with a curvature of 380 mm and a diameter of 200 mm with 2343 2 mm holes. Another lens is a plano-convex shaped lens with a curvature of 73 mm and a diameter of 72, and 253 2 mm holes. This relay lens is capable of focusing a beam width of ~38 mm. The beam width of the probing beam is measured on a test bench. Figure 6 shows the beam profile obtained with a sub-THz imaging camera (TeraSense T30, 64 × 64 pixel^2), where the beam width is less than 40 mm at the 3 m distance. In addition, remote beam steering is possible, and a scattering angle of 159° ± 6° can be realized, covering almost the entire plasma radius.

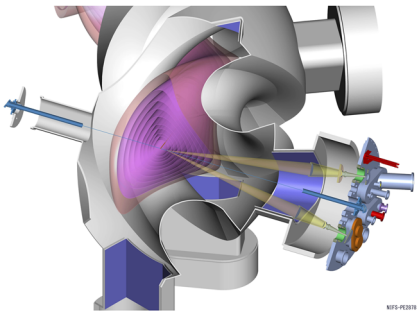

FIG. 4. Three-dimensional LHD CAD design of an in-vessel antenna pair for the back-scattering system. Here, the plasma shape is illustrated by the magnetic surface layers (pink).

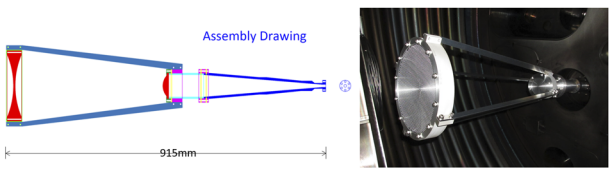

FIG. 5. Drawing of the metal lens combination antenna (left) and the photograph of the installation in-vessel of LHD (right).

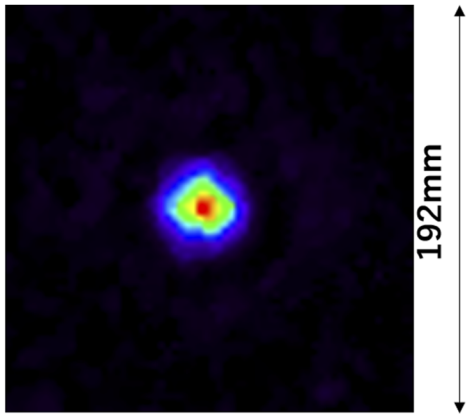

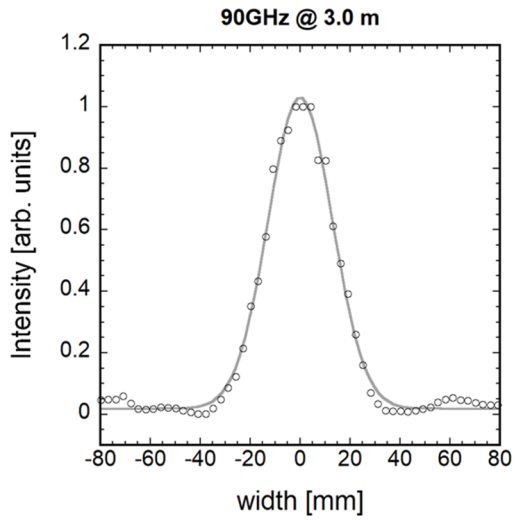

FIG. 6. Beam profile pattern at the focusing point of 3 m distant from the antenna (upper) and the profile sliced on the center line of left figure (bottom).

III. MILLIMETER WAVE CIRCUIT

The millimeter wave circuit for the back-scattering measurements is shown in Fig. 7. Since precise density fluctuation measurements require the low-noise source for probing beam, a dielectric resonator oscillator with a synchronized quartz oscillator is used as a source. Probing 90 GHz millimeter wave is generated by ×6 multipliers. A part of the probe 15.0 GHz wave is led to the mixer (mixer 1) and mixed with the local 15.15 GHz wave to generate the intermediate frequency (IF) component for heterodyne phase measurements. In the W-band mixer (mixer 2), the received 90 GHz wave and the local 90.9 GHz wave are mixed to generate another IF signal component. Each IF signal is used for quadrature signal detection, and the output of in/quadrature (IQ) detection is led to the analog to digital convertors (National Instruments PXI-6115) with a sampling rate of 2.5 MHz. The LABCOM data acquisition system collects the acquired signal in real-time and also controls the acquisition setting via their web site.[25] In addition, the above millimeter wave circuits are located in the diagnostic room, which is separated from the LHD experiment room. Because of the need to connect the 60 m distance

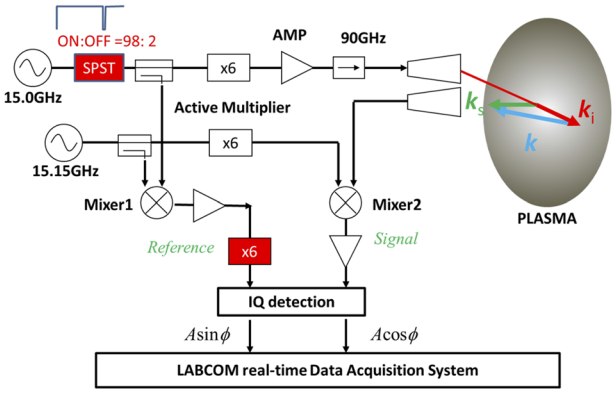

FIG. 7. Schematic of the W-band 90 GHz millimeter wave circuit for the back-scattering measurements. Two synchronized oscillators are used as a source. Active ×6 multipliers provide from the oscillator frequencies to the W-band millimeter waves. The power of the probe wave is modulated by a Single Pole Single Throw (SPST) switch for the estimation of background noise. A local oscillator is used for heterodyne detection. Two intermediate frequency (IF) components, which are indicated as "*Reference*" and "*Signal*," are generated in each mixer. Each IF signal is used for quadrature signal detection. The output of IQ detection is fed to the 2.5 MHz data acquisition system in real-time (LABCOM data acquisition system). In addition, this millimeter wave system is located at the diagnostic room and the 60 m corrugated waveguides (not shown here) connect to the viewing port.

with low transmission loss, 1.5 and 3.0 in. corrugated waveguides are used to connect to the LHD viewing port. The measured transmission loss is shown in Fig. 8. The total transmission loss is ~8 dB at 90 GHz. This value includes the losses due to two quartz windows and 12 miter bends.

In the current configuration, the main noise is considered to be ECE radiation. In order to estimate the noise level during the

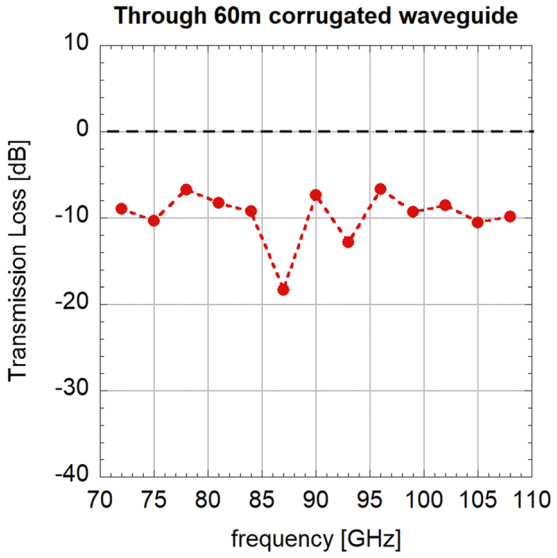

FIG. 8. *In situ* transmission loss measurement of 1.5-in. corrugated waveguide. Note that this result includes two quartz windows and 12 bends.

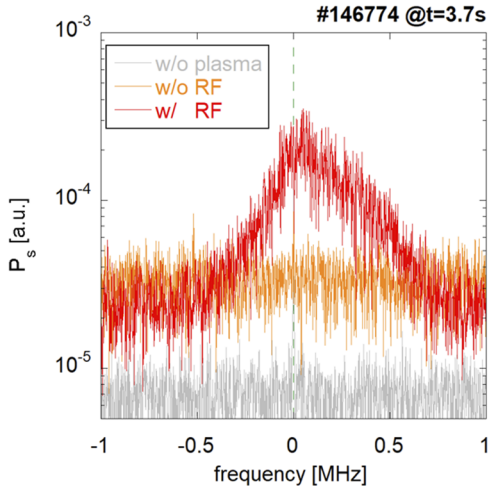

FIG. 9. Complex frequency power spectrum of the scattering signal from the plasma (red). The "w/o RF" line (gray) indicates the system noise level, and the "w/o RF" line (orange) shows the background plasma noise, which is considered to be mainly radiated ECE.

plasma discharge, the system is modified to modulate the power of a probe wave with a single pole single throw (SPST) switch. When the SPST switch is off, the probe beam does not launch to the plasma and only ECE radiation noise can be detected. Figure 9 shows the observed frequency spectrum. ECE radiation noise, which has broad frequency components, is detected, but the scattered signal is found to be large enough to allow the fluctuation measurements. In addition, the case of the spectrum of "w/o plasma" shows the small intensity. This means the reflected wave components from the opposite wall, that is, multi-reflection components, are small. Currently, during normal plasma measurements, SPST operates at a ratio of 98 (on): 2 (off) to estimate the background noise. Therefore, the high wavenumber turbulence is routinely observed by this back-scattering system.

In the current antenna setup (Fig. 4), the radial component of the perpendicular wavenumber is dominant. Theoretically, the large poloidal wavenumber is of more interest for ETG studies. However, we think both radial and poloidal components are not independent and the radial wavenumber measurement is meaningful. Simulations involving both components allow for comparison study to be made. Since it is important to know this wavevector information, scattering position, and beam bending effects, the LHDGauss ray tracing code[26,27] on the AutoAna system[28] is used to analyze the experimental conditions immediately after each LHD plasma discharge.

ACKNOWLEDGMENTS

The authors would like to thank the technical staff of LHD for their support. The authors also would like to thank Mrs. K. Takehara and T. Ito for their support of metallic lens production. This work was partially supported, in part, by KAKENHI (Grant Nos. 19H01880, 17K18773, 17H01368, 15H02335, and 15H02336), by a budgetary grant-in-aid from the NIFS LHD

project under the auspices of the NIFS Collaboration Research Program (Grant Nos. ULPP027 and KLPH024), by the NINS program for cross-disciplinary study (Grant Nos. 01311802 and 01311903), and by the collaboration programs of the RIAM of Kyushu University and FIR-UF of Fukui University. Additional support was provided by Japan/U.S. Cooperation in Fusion Research and Development.

DATA AVAILABILITY

The data that support the findings of this study are available from the corresponding author upon reasonable request.

REFERENCES

[1]T. Tokuzawa, Nucl. Fusion **57**, 025001 (2017).
[2]S.-I. Itoh and K. Itoh, Plasma Phys. Controlled Fusion **43**, 1055 (2001).
[3]J. Li and Y. Kishimoto, Phys. Rev. Lett. **89**, 115002 (2002).
[4]C. Holland and P. H. Diamond, Phys. Plasmas **11**, 1043 (2004).
[5]J. Candy *et al.*, Plasma Phys. Controlled Fusion **49**, 1209 (2007).
[6]T. Görler and F. Jenko, Phys. Rev. Lett. **100**, 185002 (2008).
[7]N. Bonanomi, P. Mantica *et al.*, Nucl. Fusion **58**, 124003 (2018).
[8]S. Maeyama, Y. Idomura *et al.*, Phys. Rev. Lett. **114**, 255002 (2015).
[9]Y. Ren, W. X. Wang *et al.*, Phys. Plasmas **22**, 110701 (2015).
[10]E. Mazzucato, D. R. Smith *et al.*, Phys. Rev. Lett. **101**, 075001 (2008).
[11]T. L. Rhodes *et al.*, Rev. Sci. Instrum. **77**, 10E922 (2006).
[12]W. Lee, H. K. Park *et al.*, Rev. Sci. Instrum. **87**, 043501 (2016).
[13]J. C. Hillesheim, N. A. Crocker *et al.*, Nucl. Fusion **55**, 073024 (2015).
[14]R. Barchfeld, C. W. Domier *et al.*, Rev. Sci. Instrum. **89**, 10C114 (2018).
[15]Y. Takeiri, T. Morisaki *et al.*, Nucl. Fusion **57**, 102023 (2017).
[16]K. Tanaka, C. A. Michael *et al.*, Rev. Sci. Instrum. **79**, 10E702 (2008).
[17]T. Tokuzawa, H. Tsuchiya *et al.*, Rev. Sci. Instrum. **89**, 10H118 (2018).
[18]T. Kobayashi *et al.*, Plasma Phys. Controlled Fusion **62**, 125011 (2020).
[19]M. Nunami, T.-H. Watanabe *et al.*, Plasma Fusion Res. **5**, 016 (2010).
[20]M. Nunami *et al.*, Plasma Phys. Controlled Fusion **59**, 044013 (2017).
[21]K. Tanaka, K. Nagaoka *et al.*, Nucl. Fusion **57**, 116005 (2017).
[22]K. Tanaka *et al.*, Plasma Phys. Controlled Fusion **62**, 024006 (2020).
[23]M. Nakata *et al.*, Plasma Phys. Controlled Fusion **61**, 014016 (2019).
[24]D. H. Froula, S. H. Glenzer, N. C. Luhmann, Jr., and J. Sheffield, *Plasma Scattering of Electromagnetic Radiation* (Academic Press, 2011).
[25]H. Nakanishi, M. Ohsuna *et al.*, IEEE Trans. Nucl. Sci. **63**, 222 (2016).
[26]S. Kubo *et al.*, "ECH power deposition study in the collisonless plasma of LHD," AIP Conf. Proc. **669**, 187 (2003).
[27]T. Ii Tsujimura *et al.*, Nucl. Fusion **55**, 123019 (2015).
[28]M. Emoto, K. Ida, C. Suzuki *et al.*, Fusion Eng. Des. **89**, 758 (2014).